J Inorg Organomet Polym (2015) 25:126–132
DOI 10.1007/s10904-014-0111-3

Photo- and Electro- Switchable Hybrid Assembly of Redox-Active Polyoxometalates and Block Copolymers

Yang Liu · Hongxiang Zhao · Haibing Wei · Nan Shi · Jie Zhang · Xinhua Wan

Received: 27 August 2014 / Accepted: 15 October 2014 / Published online: 26 October 2014

Abstract The hybrid assembled materials based on redox-active polyoxometalates $H_3PMo_{12}O_{40}{\cdot}nH_2O$ and the neutral–cationic block copolymers poly(ethylene oxide-block-*N*,*N*-dimethylaminoethyl methacrylate) in aqueous solution were constructed through electrostatic interactions. Triggered by photochemical or electrochemical methods, the charge number of the redox-active polyoxometalates charged in situ, which not only induced the chromisity of the solution, but also driven diverse morphologies of the assembly. The assembly morphologies could be switched between spherical micelles and worm-like micelles after extra stimuli. Both of chromic and assembling processes are reversible and repeatable. Moreover, the hybrid materials improve the processability of the inorganic cluster polyoxometalates which maintains its original chromic properties at the same time. This simple strategy put a general way to fabricate smart stimuli-responsive polyoxometalates-based functional materials with potential applications in optical switches, biosensors, detectors and electrochromic devices. The variety of the ionic inorganic clusters and polyelectrolytes offered a broaden platform to enrich the electrostatic-motivated assembling and expand their applications.

Y. Liu · H. Zhao · H. Wei · N. Shi · J. Zhang (✉) · X. Wan (✉)
Beijing National Laboratory for Molecular Sciences, Key Laboratory of Polymer Chemistry and Physics of Ministry of Education, College of Chemistry and Molecular Engineering, Peking University, Beijing 100871, China
e-mail: jz10@pku.edu.cn

X. Wan
e-mail: xhwan@pku.edu.cn

Keywords Photochromic · Electrochromic · Hybrid assembly · Block copolymer · Polyoxometalates

1 Introduction

Fabrication of smart materials by multiple building blocks through self-assembly strategies is emerging as a powerful approach for integration of functionalities in materials science [1–4]. Smart materials can undergo reversible chemical or physical changes under external stimuli, such as light, electric, chemical reagents, pH, and temperature, resulting in modulated supramolecular structures and functions. Incorporation of inorganic materials into hybrid responsive assembling system could significantly improve the performance of the smart materials due to their extraordinary functionalities. However, it is still challenging that how to master the self-assembly capability of the inorganic particles as well as the responsive properties to achieve hierarchical structures [5–7]. Polyoxometalates (POMs) are a type of giant inorganic transition metal oxide clusters on the nanoscale with diverse catalytic, electro-optical, and biological properties [8–12]. Besides covalent modification of POM clusters with organic building blocks [13–19], efforts also have been made to fabricate core–shell hybrid assemblies of POMs with cationic surfactants [20–23] or polymers [24–29] driven by electrostatic interactions. The polymers not only act as ideal protective matrices for POMs, but also greatly enhance functionalities of POM. [29] On the other hand, POMs with adjustable charges could be utilized to facilely modulate morphologies of the block copolymers (BCPs) [24–29].

Herein, we construct the in situ photo- and electro-responsive hybrid assembled materials based on the redox-active POM $H_3PMo_{12}O_{40}{\cdot}nH_2O$ (PMo_{12}) and the BCPs,

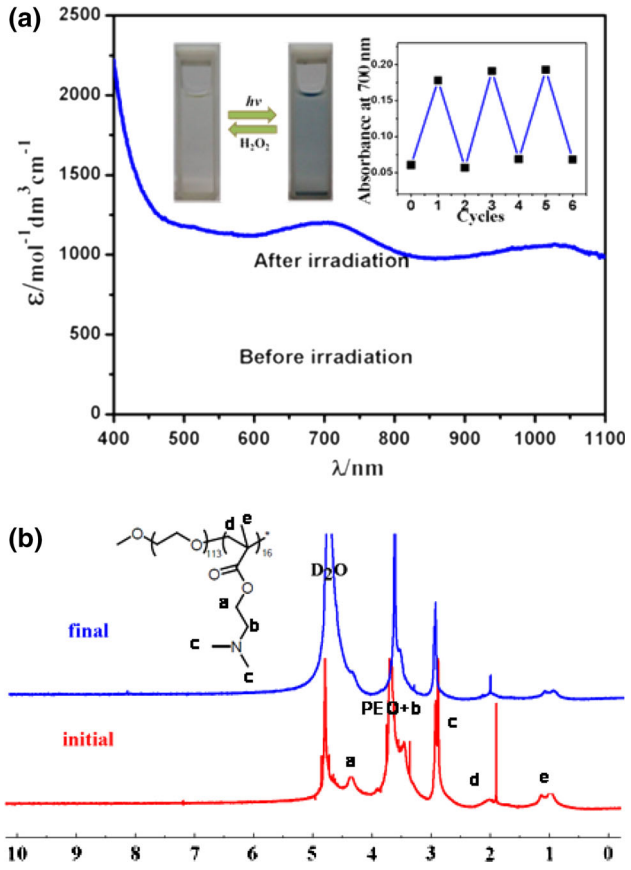

Fig. 1 **a** UV absorption spectra and photographs of PMo_{12}-BCP complex solution before and after irradiation for 1 h. The *inset* figure: photochromic cycles by the irradiation of UV light and following oxidization by H_2O_2, collected by UV/Vis absorption at 700 nm. **b** ^1H NMR spectra of BCP in D_2O before (*red*) and after (*blue*) adding H_2O_2 (Color figure online)

poly(ethylene oxide-block-*N*,*N*-dimethylaminoethyl methacrylate) (PEO_{113}-*b*-$PDMAEMA_{16}$). In acidic aqueous solution, the anionic PMo_{12} complex with the cationic segment of protonated PDMAEMA through electrostatic interactions to assemble into the ionic core, stabilized by the neutral shell of the hydrophilic PEO segment. PMo_{12} itself is redox-active, i.e., the heteropolyacid (HPA) state of PMo_{12} can be facilely reduced to the heteropolyblue (HPB) state in blue color under irradiation of light and then be recovered in the presence of H_2O_2 [30]. The reduced HPB state of PMo_{12} carries more negative charges than the HPA state, which means that the charge density of PMo_{12} is reversibly adjustable during the redox process while the architecture of the cluster almost remains intact [31–33]. Therefore, it is expected that such an in situ adjustment of charge density of PMo_{12} during the redox process may further modulate the electrostatic interactions between PMo_{12} and BCP, resulting in the morphological switching of hybrid assemblies [34]. Besides, PMo_{12} is a good candidate for constructing stimuli-responsive systems because both of the oxidized state HPA and the reduced state HPB are stable in air, prior to the analogue $H_3PW_{12}O_{40}$ of which the fast bleaching occurs in the air [35–37]. We could readily observe the morphological modulation of the hybrid PMo_{12}-BCP complex in both stable states.

In the present work, the micellar solutions were prepared at a stoichiometric charge ratio of the PMo_{12} anions to the ammonium cations of the hydrophilic BCP. The nano-assemblies of the HPA–BCP hybrid complex were visualized by using transmission electron microscopy (TEM). Spherical micelles with an average diameter of $\sim$10 nm were observed, as shown in Fig. 1a, b. The elementary analysis of the spherical assemblies by TEM energy dispersive X-ray (EDX) confirms the presence of Mo from HPA and N from BCP (Fig. 2i).

2 Experimental

2.1 Materials

The polyoxometalate $H_3PMo_{12}O_{40}{\cdot}nH_2O$ was purchased from Alfa Aesar and the block copolymer PEO_{114}-*b*-$PDMAEMA_{16}$ (PDI = 1.2) was purchased from Polymer Source, Canada, and used as obtained. Lithium bis(trifluoromethane sulfonimide) ($LiNTf_2$) and Isopropenyl acetate (IPC) were purchased from J&K. Polymethylmethacrylate (PMMA) and acetonitrile (ACN) were of analytical grade and used without further purification.

2.2 Methods

TEM images were obtained on a JEM-2100 operating at an acceleration voltage of 200 kV. A drop of the sample solution was deposited onto a carbon-coated copper EM grid for a few minutes. Excess solutions were blotted away with a strip of filter paper, and the sample grid was dried in air.

Cyclic voltammograms (CV) were recorded on a CHI 840C electrochemical workstation. The POM solutions were made in H_2O and were deoxygenated with nitrogen prior to electrochemical work. Glassy carbon working and platinum counter electrodes were employed together with a silver pseudoreference electrode. All the electrochemical measurements were referenced to Ag/AgCl. Spectroelectrochemical data were obtained on a Perkin–Elmer lambda 35 spectrophotometer connected to a computer in an optical transparent thin layer cell. The redox potentials were chosen according to the results of CV.

Optical switching properties were monitored in a one-layer electrochromic device containing POM-BCP assemblies. The assemblies were collected from suspension of concentrated POM (1 mg/mL)-BCP micellar solution by

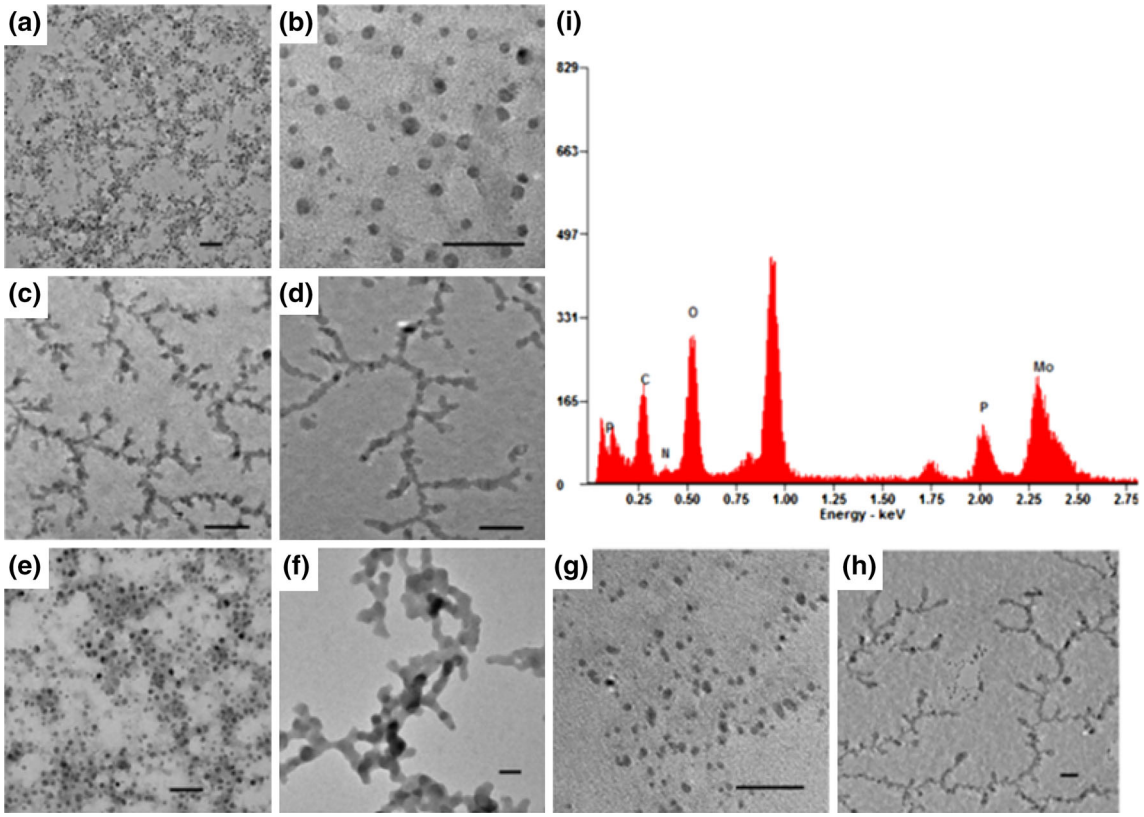

Fig. 2 TEM images of **a**, **b** initial HPA–BCP complexes; **c**, **d** HPB-BCP complexes after UV irradiation; **e** HPA–BCP complexes after five photochemical redox cycles; **f** HPB-BCP complexes after five photochemical redox cycles; **g** HPA–BCP complexes and **h** HPB–BCP complexes during the first electrochemical redox cycles. All *scale bars* are 50 nm. **i** Energy dispersive X-ray (EDX) microanalysis of the initial HPA–BCP spherical assemblies

centrifugation on a BECKMAN GS-15R refrigerated centrifuge. Then the mixture of assemblies and a solid electrolyte gel (ACN:PMMA:IPC:$LiNTf_2$ = 70:7:20:3[m%]) were coated on an ITO glass respectively. Another ITO glass was put on the film and the whole device was dried under vacuum for 24 h. The redox potentials were chosen according to the results of CV. The X-ray photoelectron spectra (XPS) of the POM-BCP films were recorded on an Axis Ultra Imaging Photoelectron Spectrometer using monochromatic Al K (1,486.6 eV) radiation. The instrument resolution was about 0.48 eV.

3 Results and Discussion

The redox properties of PMo_{12} in the obtained HPA–BCP complex were investigated through the photochemical methods. After 1 h of irradiation with UV light ($\lambda = 254$ nm), the clear and colorless solution turns turbid blue. The typical absorption spectra of the solution before and after photo-irradiation are shown in Fig. 1. The new broad absorption band centered at 699 nm could be assigned to the Mo(V) → Mo(VI) intervalence charge transfer (IVCT), revealing that HPA PMo_{12} molecules have been reduced to HPB accompanied by the coloration process. The XPS of dried samples (Fig. 3c) also confirmed the existence of Mo(V) in the blue turbid solution. Determined from the peak area ratio of Mo(VI) and Mo(V), ca. 19.7 % of Mo(VI) have been reduced to Mo(V). The HPB-BCP solution is quite stable in air and there is no decoloration in several weeks after removal of the photo-irradiation, while those turbid solutions tend to precipitate. HPB can be further reoxidized to the HPA state in the presence of H_2O_2. After about 10 μL 30 % H_2O_2 solution was added, the blue turbid solution (∼3 mL) decolored to a clear colorless solution within a couple of minutes, and even precipitates were completely redissolved. To exclude the possibility that the tertiary amine residues of the block copolymer may be oxidized by H_2O_2 during the procedure, 1H NMR of the complex in D_2O after addition of H_2O_2 was carried out. The result as shown in Fig. 1b shows that the BCP remains intact during the oxidation. The UV–Vis spectrum of the solution was almost the same with the initial HPA–BCP solution, suggesting that Mo(V) has been completely reoxidized to Mo(VI). The color change of the

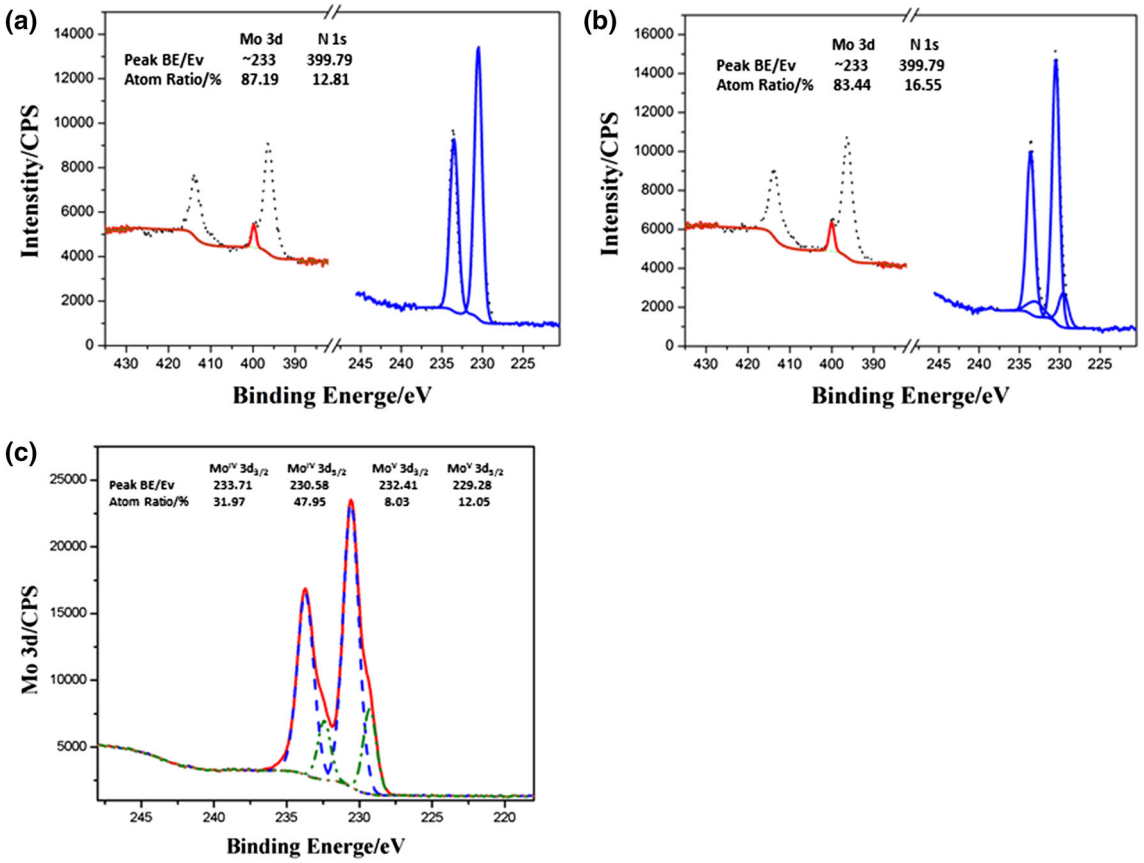

Fig. 3 XPS of the Mo 3d, N 1s photoelectron lines for the HPA–BCP assemblies solution **a** before and **b** after irradiation with UV light; **c** the XPS of the Mo $3d_{5/2,\ 3/2}$ photoelectron lines for the HPA–BCP assemblies solution after irradiation with UV light

complex solution displays good reversibility, and the coloration-decoloration cycles can repeat over several times.

The morphologies of the hybrid complex during the redox cycles have been observed by TEM (Fig. 2c, d). Interestingly, the morphological transition was induced from spherical micelles to branched wormlike micelles when HPA has been reduced to HPB under UV irradiation. The wormlike micelles have a branched structure with an average diameter of ~10 nm, which is consistent with the diameter of spherical micelles of HPA–BCP complexes (Fig. 2a, b). The TEM images show that the wormlike micelles of the complexes return to the spherical micelles (~10 nm) after oxidization with H_2O_2. After five photochemical redox cycles with alternative UV irradiation and H_2O_2 treatments, the morphological change is completely reversible, as shown in Fig. 2e, f. The extended length of the PDMAEMA block is estimated to be 4.0 nm, and that of the PEO block is 40.5 nm. Under TEM observation, the micelles has a average diameter of ~10 nm, indicating the PEO corona become invisible and the visible part in TEM may contain only the dense complex coacervate core of PDMAEMA/POM.

The mechanism of the photochemical reduction from HPA to HPB has been well described previously in the literature [35]. In brief, crystal structural studies of Keggin-type reduction species under photo-irradiation reveal that there are a two-electron reduction species α-$[HPMo_{12}O_{40}]^{4-}$ and a four-electron reduction species β-$[H_4PMo_{12}O_{40}]^{3-}$ [35, 36]. According to XPS results that 19.7 % of Mo(VI) have been reduced to Mo(V) (Fig. 3c), it could be further deduced that the reduced product contains 80 % of two-electron reduction species α-$[HPMo_{12}O_{40}]^{4-}$ and 20 % of four-electron reduction species β-$[H_4PMo_{12}O_{40}]^{3-}$. α-$[HPMo_{12}O_{40}]^{4-}$ carries 4 negative charges, more than 3 negative charges of HPA. Zeta potential of the HPB-BCP complex is -31.25 ± 0.97 mV while that of the HPA–BCP complex is -18.25 ± 1.26 mV, indicating that HPB complexes took more negative charges than HPA complexes. Further XPS analysis as shown in Fig. 3a, b reveals that the *N* content in the nano-assemblies slightly increase from 12 to 16 % after UV irradiation, indicating that more free BCPs chains were involved into the HPB-BCP complex than the HPA–BCP complex. Based on above evidences,

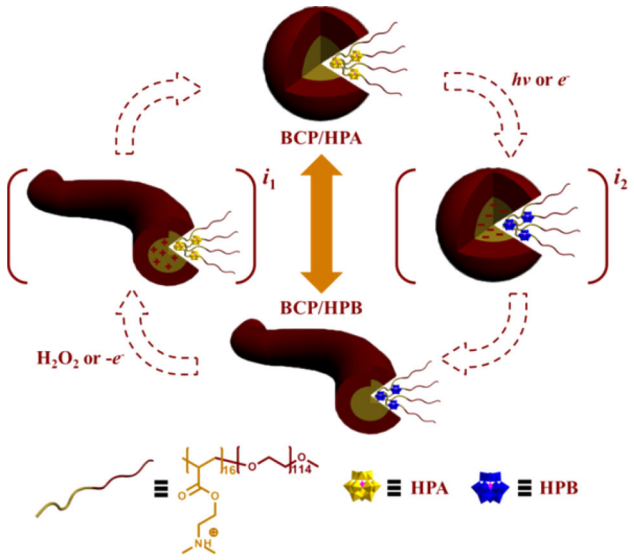

Scheme 1 Schematic illustration of the reversible redox-modulated morphological transitions of hybrid assembly of BCP/HPA and BCP/HPB. The possible intermediates, negatively charged BCP/HPB spheres and positively charged BCP/HPA wormlike micelles, are denoted as i1 and i2 in the parentheses

we propose the possible mechanism of the morphological transition (Scheme 1): At the initial state, anionic HPA complex with the cationic PDMEAMA segment of PEO-*b*-PDMEAMA BCPs to form ionic core of spherical micelles which are negatively charged according to the negative values of zeta potential measurement. As HPA was reduced to HPB under photo-irradiation, the ionic core of the spherical micelles becomes significantly negatively overcharged. To partially neutralize the extra charges, some free cationic BCP chains in solution would insert into the cores of spherical micelles. Therefore the expanded relative hydrophobic contents in the core–shell superstructures triggered the evolution from spherical micelles to the more thermodynamically stable wormlike micelles. Such a spherical-to-wormlike micellar transition induced by increasing the relative hydrophobic fractions is frequently observed in the assembling system of amphiphilic BCPs. [38, 39] Due to the slow chain mobility of polyelectrolytes, the proposed easiest way is that the spherical micelles were glued by the additional BCPs and lead to the formation of wormlike micelles. That explains that the branched wormlike micelles seem to originate from the interconnected spherical micelles. As HPB was oxidized to HPA by H_2O_2, the wormlike micelles become less negatively charged. To revert to the original state, some cationic BCPs may be "squeezed" out of the wormlike micelles, followed by the evolution into spherical particles. The redox-modulated morphology of the hybrid assemblies may be attributed to the in situ adjustable charge density of PMo_{12} and the consequent tunable electrostatic interaction between PMo_{12} and BCP.

The POM-BCP assemblies in solution display electro-switchable behaviour similar to photo-triggered morphological transformation. Figure 4a shows the CV of the complex solution of HPA–BCP in water. The three redox couples were observed in the negative potential region corresponding to the two, four and six electron reduction process from Mo(VI) to Mo(V) [40]. The absorption spectra of the complex in the first two reduction states at different potentials are shown in Fig. 4b. The initial HPA–BCP complex displays almost no absorbance at above 500 nm. Electrochemical reduction to the first two-electron state results in the appearance of a strong and broad IVCT band from 500 to 1,100 nm. At the further four-electron reduction state, the absorption above 500 nm becomes stronger especially for the band at 860 nm. The reversible electrochemical redox in solution was carried out with the applied voltage of −0.2 to −0.3 V to maintain the two-electron reduction state. TEM observation as shown in Fig. 2g, h reveals that there are spherical micelles in the oxidized HPA state and wormlike micelles in the reduced HPB state, which are very similar to previous results through photochemical redox procedure. These results indicate that electrochemical methods could also modulate the morphological transition of the POM-BCP hybrid complex.

The optical attenuation of the complex thin films cast from the aqueous solution was recorded at one of the NIR wavelength of 700 nm with stepping potentials between −0.2 and +0.2 V. (Fig. 4c). The color change of the hybrid film is reversible, and the coloration-decoloration cycles can repeat over ten times, implying highly photochromic stability and potential applications in the field of photoswitches and memory devices in the visible and near infrared region.

4 Conclusions

In summary, we report the switchable hybrid assemblies of the POM $H_3PMo_{12}O_{40}$ and hydrophilic block copolymer PEO-*b*-PDMEAMA driven by electrostatic interactions in aqueous solutions. The micellar morphologies could be reversibly transformed between spherical micelles and wormlike micelles, triggered by multi-stimuli, i.e. UV photo-irradiation and then H_2O_2, or electrochemical methods repeatedly. Such a morphological modulation is closely related to the charge variation of PMo_{12} during the in situ redox process. Moreover, from a point view of practical applications, the hybrid materials improve the processability of the inorganic cluster PMo_{12} without loss of its good chromic properties. The present strategy paves a

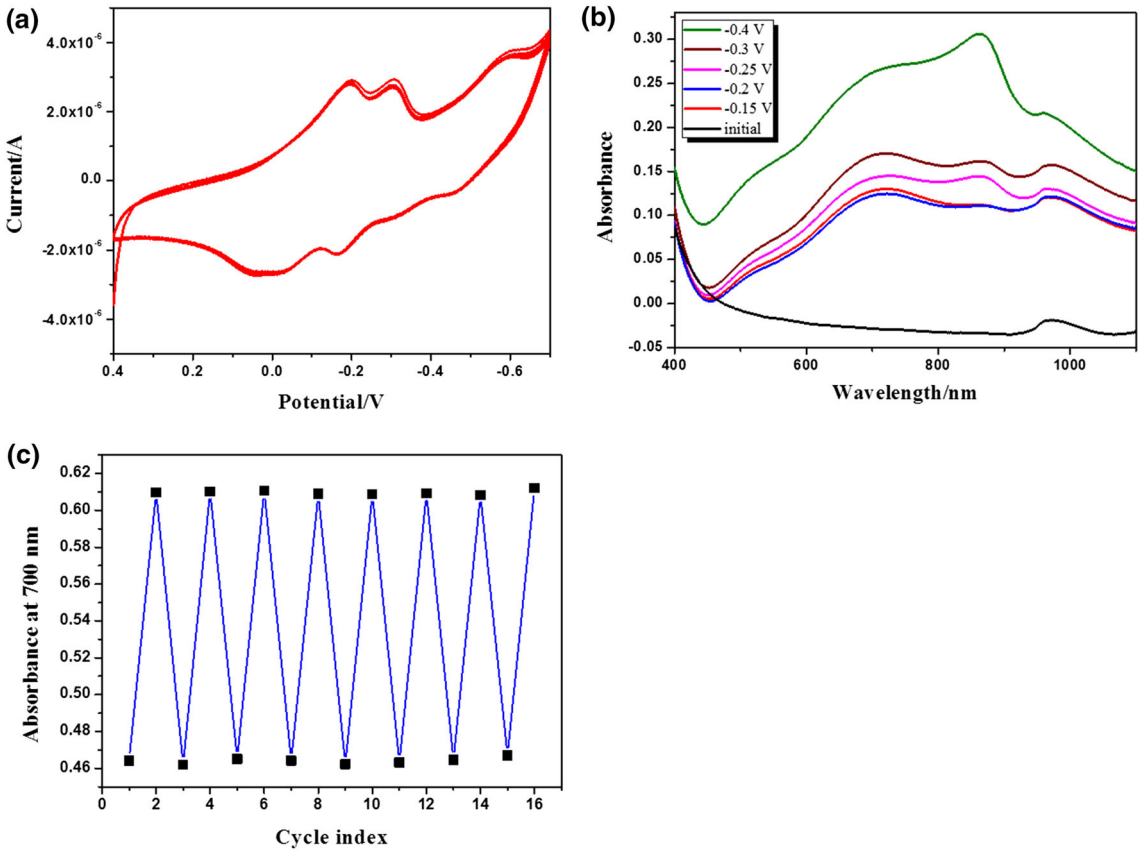

Fig. 4 Electrochromism of HPA/HPB-BCP complex. **a** Cyclic voltammograms of complex solution of HPA–BCP; **b** Absorption spectra of HPA–BCP complex at various voltages in the UV and near infrared region; **c** Optical switching of a one-layer electrochromic device containing POM-BCP assemblies with stepping potentials between −0.2 and +0.2 V. All the electrochemical measurements were referenced to Ag/AgCl

new route to fabricate smart stimuli-responsive POM-based functional materials with potential applications in optical switches, biosensors, detectors and electrochromic devices.

5 Supplementary Materials

Supplementary figures are available directly from the corresponding author or the journal editor.

Acknowledgments This work was financially supported from the Nation Science Foundation of China (No. 21322404; No. 51373001) and Beijing Natural Science Foundation (No. 2122024).

References

1. L.H. Reddy, J.L. Arias, J. Nicolas, P. Couvreur, Chem. Rev. **112**, 5818 (2012)
2. T. Fenske, H.G. Korth, A. Mohr, C. Schmuck, Chem. Eur. J. **18**, 738 (2012)
3. Q. Dai, A. Nelson, I. Tokarev, M. Motornov, S. Minko, J. Mater. Chem. **19**, 6932 (2009)
4. J. Zhang, X.F. Chen, H.B. Wei, X.H. Wan, Chem. Soc. Rev. **42**, 9127 (2013)
5. S.E. Lohse, C.J. Murphy, J. Am. Chem. Soc. **134**, 15607 (2012)
6. Y.P. Zha, H.D. Thaker, R.R. Maddikeri, S.P. Gido, M.T. Tuominen, G.N. Tew, J. Am. Chem. Soc. **134**, 14534 (2012)
7. S. Landsmann, M. Wessig, M. Schmid, H. Cöfen, S. Polarz, Angew. Chem. Int. Ed. **51**, 5995 (2012)
8. I.V. Kozhevnikov, Chem. Rev. **98**, 171 (1998)
9. N. Mizuno, M. Misono, Chem. Rev. **98**, 199 (1998)
10. A. Müller, F. Peters, M.T. Pope, D. Gatteschi, Chem. Rev. **98**, 239 (1998)
11. J.T. Rhule, C.L. Hill, D.A. Judd, R.F. Schinazi, Chem. Rev. **98**, 327 (1998)
12. A. Dolbecq, E. Dumas, C.R. Mayer, P. Mialane, Chem. Rev. **110**, 6009 (2010)
13. Y.K. Han, Y. Xiao, Z.J. Zhang, B. Liu, P. Zheng, S.J. He, W. Wang, Macromolecules **42**, 6543 (2009)
14. J. Rieger, T. Antoun, S.H. Lee, M. Chenal, G. Pembouong, J. Lesage de LaHaye, I. Azcarate, B. Hasenknopf, E. Lacôte, Chem. Eur. J. **18**, 3355 (2012)
15. D. Li, J. Song, P.C. Yin, S. Simotwo, A.J. Bassler, Y. Aung, J. Roberts, K.I. Hardcastle, C.L. Hill, T.B. Liu, J. Am. Chem. Soc. **133**, 14010 (2011)
16. J. Zhang, Y.F. Song, L. Cronin, T.B. Liu, J. Am. Chem. Soc. **130**, 14408 (2008)
17. D.L. Long, R. Tsunashima, L. Cronin, Angew. Chem. Int. Ed. **49**, 1736 (2010)

18. A. Proust, B. Matt, R. Villanneau, G. Guillemot, P. Gouzerh, G. Izzet, Chem. Soc. Rev. **41**, 7605 (2012)
19. Z.H. Peng, Angew. Chem. Int. Ed. **43**, 930 (2004)
20. D. Volkmer, A. Du Chesne, D.G. Kurth, H. Schnablegger, P. Lehmann, M.J. Koop, A. Müller, J. Am. Chem. Soc. **122**, 1995 (2000)
21. Y. Yan, H.B. Wang, B. Li, G.F. Hou, Z.D. Yin, L.X. Wu, V.W.W. Yam, Angew. Chem. Int. Ed. **49**, 9233 (2010)
22. H.L. Li, H. Sun, W. Qi, M. Xu, L.X. Wu, Angew. Chem. Int. Ed. **46**, 1300 (2007)
23. X.H. Yan, P.L. Zhu, J.B. Fei, J.B. Li, Adv. Mater. **22**, 1283 (2010)
24. Q. Zhang, L.P. He, H. Wang, C. Zhang, W.S. Liu, W.F. Bu, Chem. Commun. **48**, 7067 (2012)
25. W.F. Bu, S. Uchida, N. Mizuno, Angew. Chem. Int. Ed. **48**, 8281 (2009)
26. X.K. Lin, F. Liu, H.L. Li, Y. Yan, L.H. Bi, W.F. Bu, L.X. Wu, Chem. Commun. **47**, 10019 (2011)
27. H.B. Wei, S.M. Du, Y. Liu, H.X. Zhao, C.Y. Chen, Z.B. Li, J. Lin, Y. Zhang, J. Zhang, X.H. Wan, Chem. Commun. **50**, 1447 (2014)
28. H.B. Wei, N. Shi, J.L. Zhang, Y. Guan, J. Zhang, X.H. Wan, Chem. Commun. **50**, 9333 (2014)
29. J. Zhang, Y. Liu, Y. Li, H.X. Zhao, X.H. Wan, Angew. Chem. Int. Ed. **51**, 4598 (2012)
30. T. Yamase, Chem. Rev. **98**, 307 (1998)
31. R. Neier, C. Trojanowski, R. Mattes, J. Chem. Soc., Dalton Trans. **15**, 2521 (1995)
32. J.N. Barrows, G.B. Jameson, M.T. Pope, J. Am. Chem. Soc. **107**, 1771 (1985)
33. A. Müller, E. Krickemeyer, M. Penk, V. Wittenben, J. Doring, Angew. Chem. Int. Ed. **29**, 88 (1990)
34. I.K. Voets, A. de Keizer, M.A. Cohen Stuart, Adv. Colloid Interface Sci. **147–148**, 300 (2009). and references therein
35. W. Feng, T.R. Zhang, Y. Liu, R. Lua, C. Guan, Y.Y. Zhao, J.N. Yao, Mater. Chem. Phys. **77**, 294 (2002)
36. J. Chen, W. Feng, L.L. Dong et al., J. Mol. Struct. **1049**, 414 (2013)
37. E. Ishikawa, T. Yamase, Bull. Chem. Soc. Jpn **73**, 641 (2000)
38. S. Jain, F.S. Bates, Science **300**, 460 (2003)
39. N.S. Cameron, M.K. Corbierre, A. Eisenberg, Can. J. Chem. **77**, 1311 (1999)
40. N. Tanaka, K. Unoura, E. Itabashi, Inorg. Chem. **21**, 1662 (1982)